Biophysical Journal, Volume *116*

Supplemental Information

Solvatochromic Modeling of Laurdan for Multiple Polarity Analysis of Dihydrosphingomyelin Bilayer

Nozomi Watanabe, Yuka Goto, Keishi Suga, Thomas K.M. Nyholm, J. Peter Slotte, and Hiroshi Umakoshi

Emission spectra of Laurdan in DOPC/PSM and DOPC/DHPSM bilayer

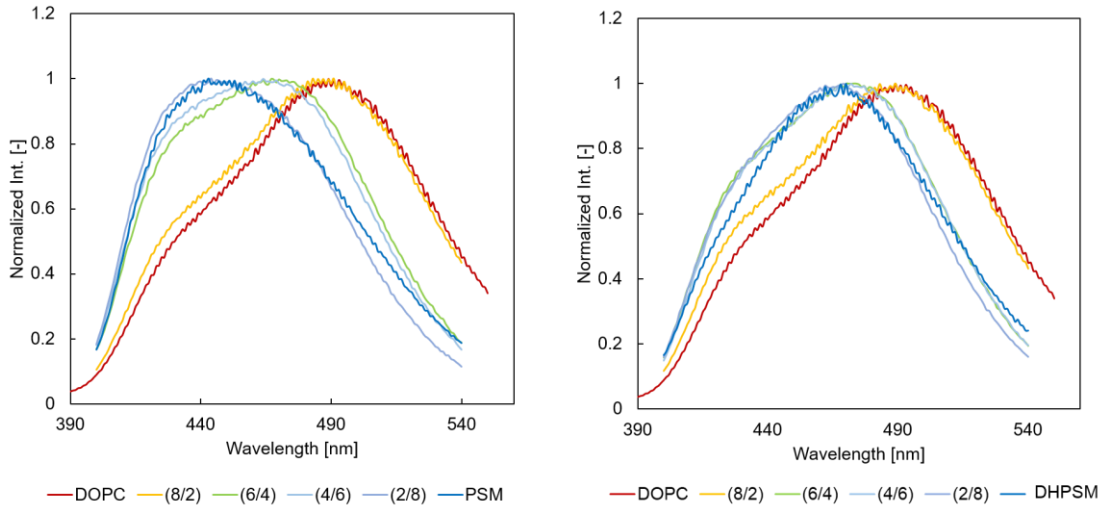

Figure S1. Fluorescence emission spectra of Laurdan in the DOPC/PSM and DOPC/DHPSM binary systems at 20 °C. The ratios of the lipid composition of DOPC, PSM, and DHPSM are written as (DOPC/PSM (or DHPSM)). The excitation wavelength is 360 nm. All spectra were normalized with the strongest peak intensity. The reproducibility was confirmed from the transition as a function of lipid composition.

Transition of the *GP* value

The generalized polarization value was measured according to a previous report (1) with the following equation:

$$GP = \frac{I_{440\ \mathrm{nm}} - I_{490\ \mathrm{nm}}}{I_{440\ \mathrm{nm}} + I_{490\ \mathrm{nm}}} \qquad \text{(Eq. S1)}$$

where $I_{440\ \mathrm{nm}}$ is the emission intensity at 440 nm in the emission spectrum of Laurdan in the steady state, and $I_{490\ \mathrm{nm}}$ is the emission intensity at 490 nm.

The *GP* values decreased with an increase in temperature. Except for DOPC, the values shifted drastically based on the transition temperature. At room temperature, *GP* values become smaller in the order of DPPC > PSM > DHPSM > DOPC, which also corresponds to the order of degree of hydration.

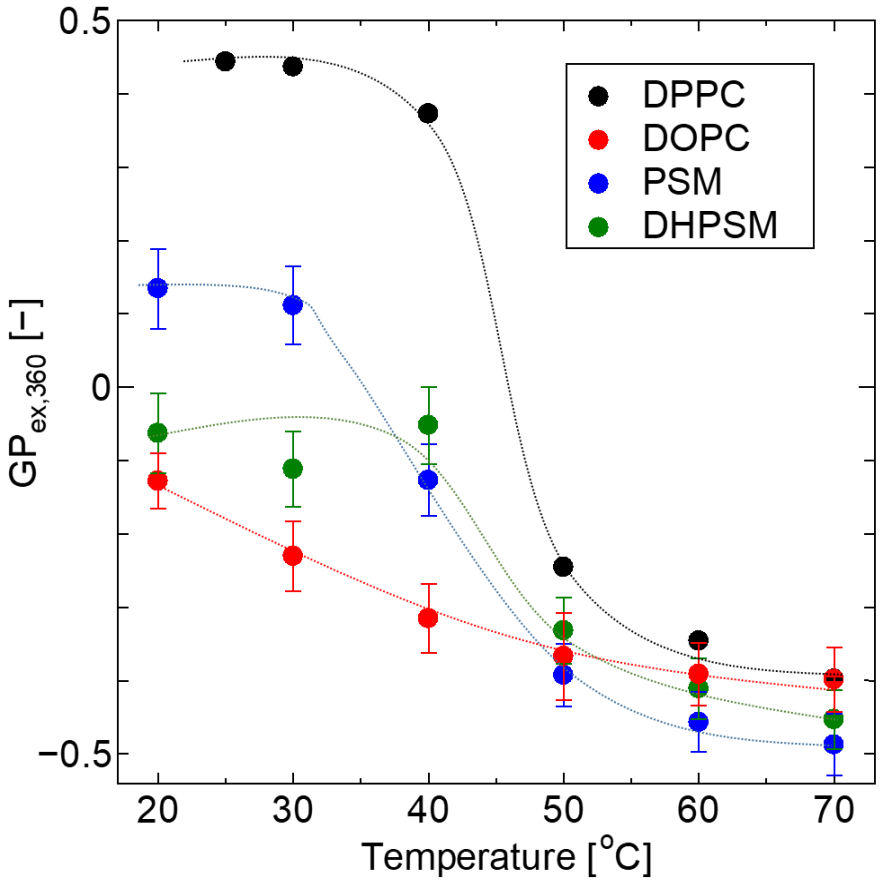

Figure S2. Transition of *GP* values in the DPPC, DOPC, PSM, and DHPSM bilayers as a function of temperature. Each lipid is depicted in the color described in the legends. The *GP* value is defined as described in Eq. S1. The average value was plotted from the *GP* values calculated from the three emission spectra shown in Figure 1. Error bars represent SEM.

Anisotropy of Laurdan in binary bilayers

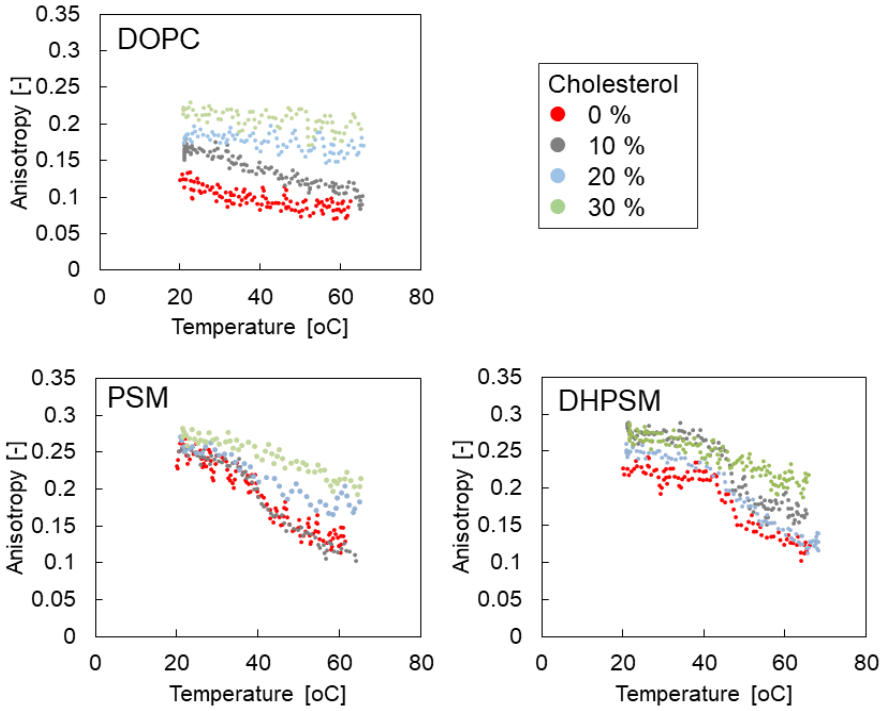

Figure S3. Anisotropy transition of Laurdan as a function of temperature observed in DOPC/cholesterol, PSM/cholesterol, and DHPSM/cholesterol binary bilayer systems. Red curves represent single component lipid bilayers, DOPC, PSM, and DHPSM, respectively. The legend shows the composition of cholesterol. The excitation wavelength were 360 nm and 490 nm for the emission. Anisotropy was measured as described in the Methods section using the Eq. 1 and 2. The reproducibility was confirmed from the transition as a function of temperature. For all samples, a large scattering was observed in the anisotropy values, which could be due to the variety of orientations in each molecular environment where Laurdan exists.

Quenching experiment with 5-DOXYL and TEMPO

Fluorescence quenching experiments were performed to reveal the multiplicity of Laurdan locations in DPPC, DOPC, PSM, and DHPSM bilayers. The spin-labeled quenchers 2-(3-carboxypropyl)4,4-dimethyl-2-tridecyl-3-oxazolidinyloxy (5-DOXYL stearic acid) and 2,2,6,6-tetramethylpiperidine 1-oxyl free radical (TEMPO) were used as a site-specific quencher and bulk-distributed quencher, respectively. According to the parallax method using l-palmitoyl-2-(5-doxyl)stearoyl-*sn*-glycero-3-phosphocholine, the distance from the bilayer center to the 5-DOXYL moiety in stearoyl chain is estimated to be 12.15 Å in DOPC bilayer (2, 3). The fluorescence would be quenched if the Laurdan molecules were located as close as they are to the radical molecules. TEMPO is a water-soluble molecule and is partitioned favorably into the disordered phase of the lipid membrane. Therefore, the penetration of TEMPO and quenching would be promoted as the increase of TEMPO concentration.

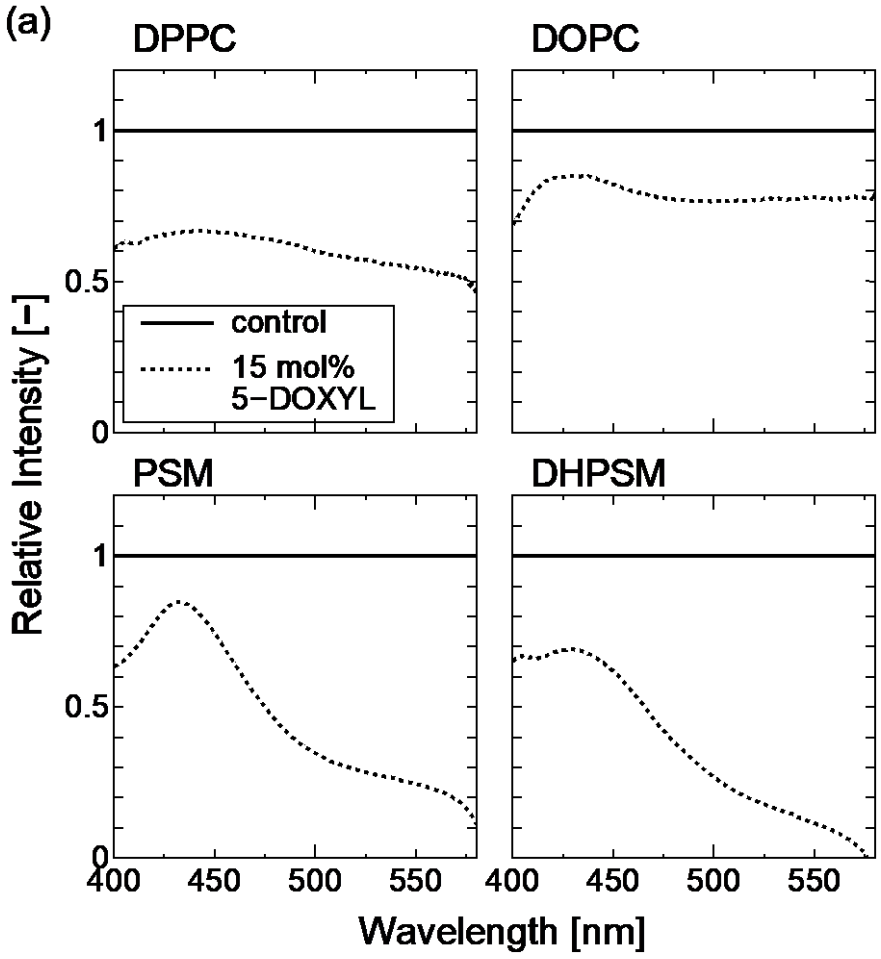

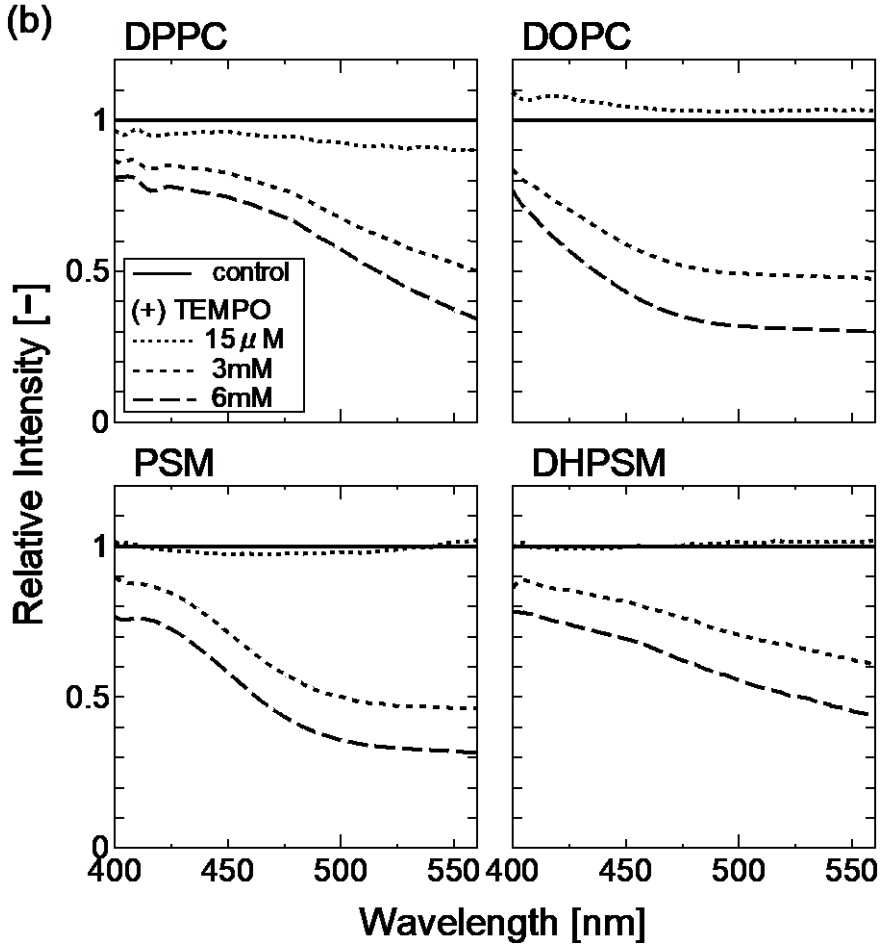

Figure S4. Relative emission intensity of Laurdan in the presence of quenchers, shown as a spectrum. The solid lines represent the emission spectra of Laurdan as a control, and the dotted lines represent the relative intensities between the spectra obtained **(a)** in the presence of 15 mol% of 5-DOXYL stearic acid and **(b)** in the presence of TEMPO. All experiments were performed with a 100-μM lipid concentration and 3 mol% of Laurdan, respectively. The emission spectra were obtained with excitation at 360 nm at 20 °C. All spectra acquisitions were repeated three times.

Center of mass of time-resolved emission spectra of Laurdan

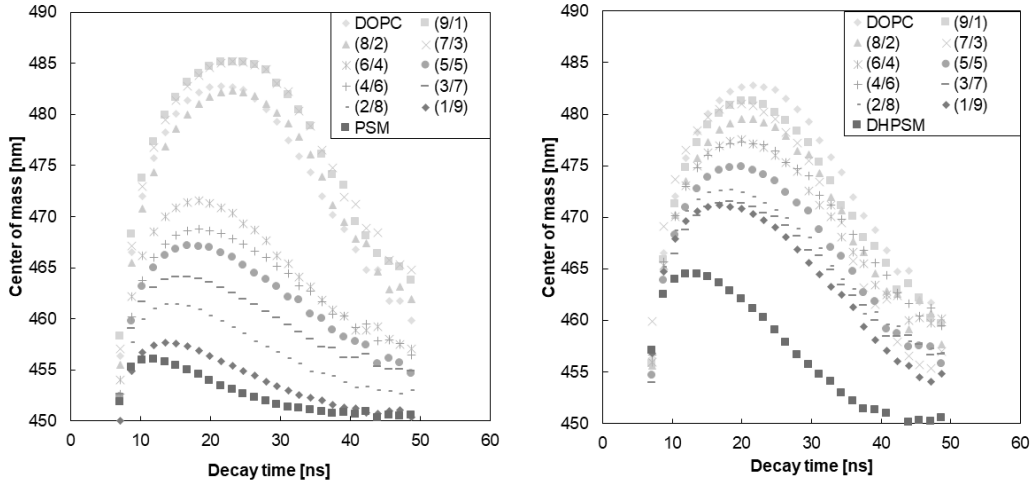

Figure S5. Center of spectral mass for each bilayer in the DOPC/PSM and DOPC/DHPSM binary systems at 20°C. The ratios of the lipid composition of DOPC, PSM, or DHPSM are written as (DOPC/PSM (or DHPSM)). The excitation wavelength of the pus laser is 378 nm. The value was calculated according to Eq. 4, and data points were extracted every 7.168 ns. The composition of PSM or DHPSM is increasing as the color gets darker. The reproducibility was confirmed from the transition as a function of lipid composition.

Excitation spectra of Laurdan

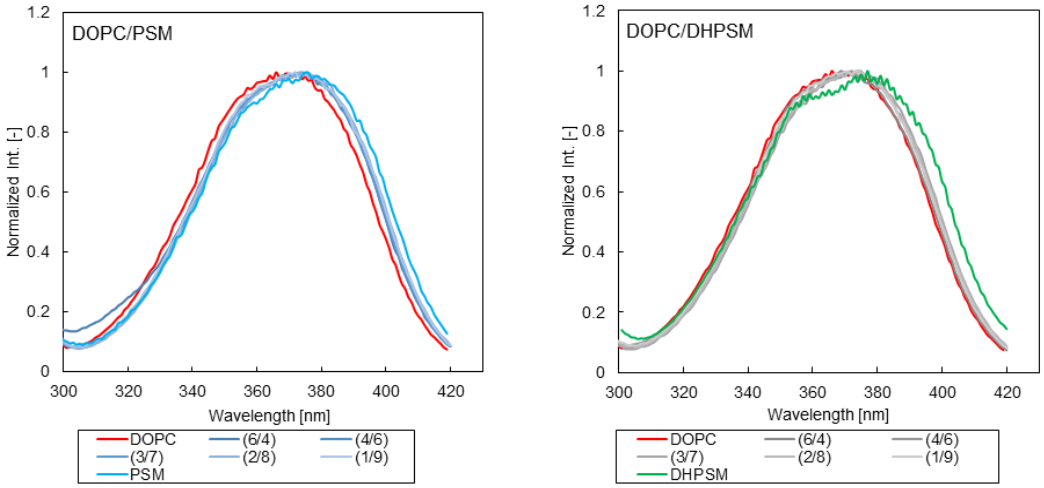

Figure S6. Excitation spectra of Laurdan in DOPC/PSM and DOPC/DHPSM bilayers, recorded at the emission wavelength of λ_{em} = 435 nm at 20 °C. The ratios of the bilayer lipids composition of DOPC, PSM or DHPSM are written in (DOPC/PSM (or DHPSM)). DOPC, PSM, and DHPSM are illustrated in the color of red, blue and green, respectively. The intermediate composition is represented by the gradient of color. All spectra were normalized with the strongest peak intensity. The reproducibility was confirmed from the transition as a function of lipid composition.

Excitation dependencies in the emission spectra

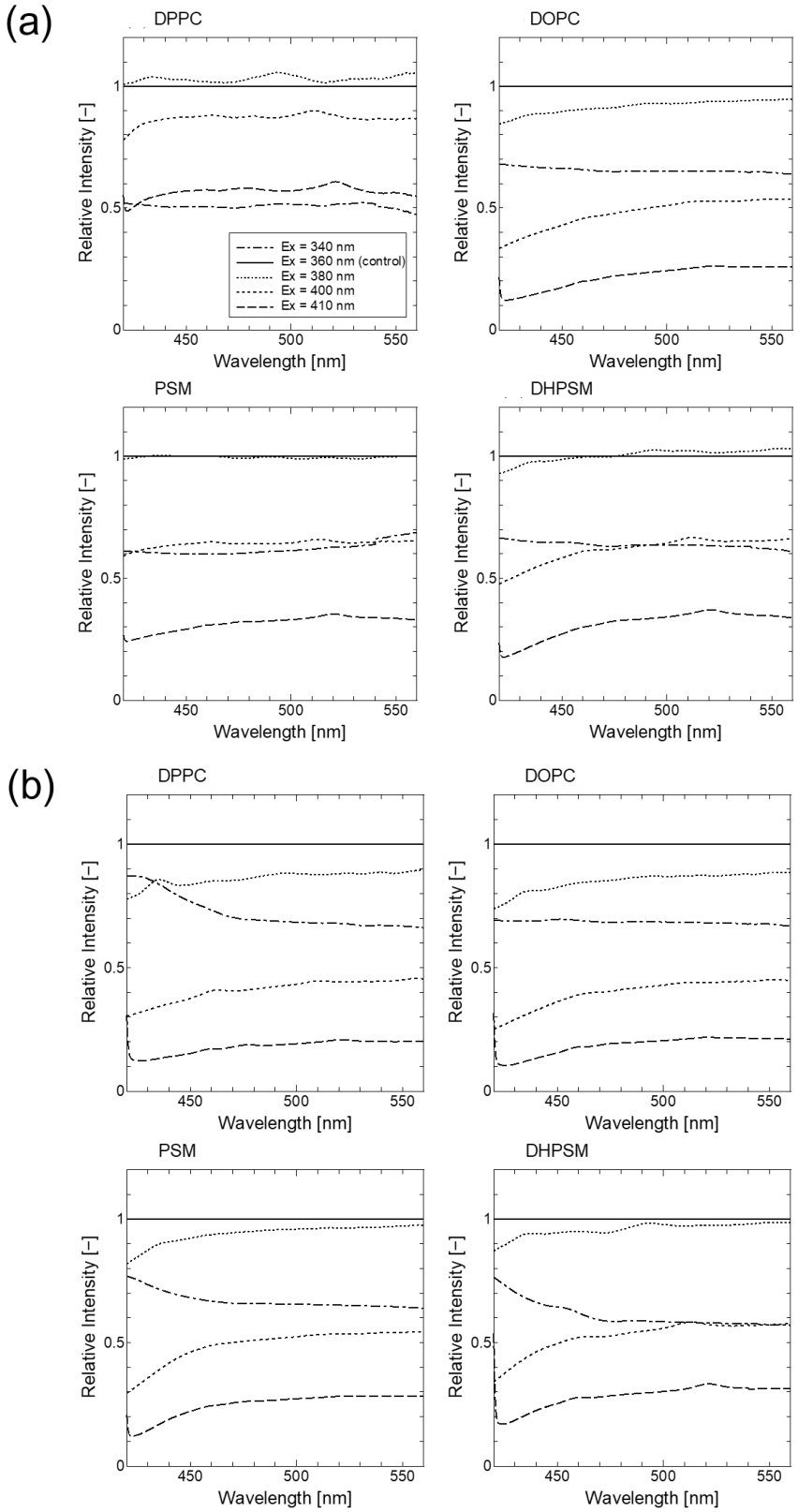

Figure S7. Ratio spectra between steady-state Laurdan emission spectra excited at various

excitation wavelengths. The results were obtained (a) at 25 °C and (b) at 60 °C. All spectra were calculated with the spectra excited at 360 nm as a control. The arbitrary excitation wavelengths are shown in the legend. The concentrations of samples were 100 μM of lipids and 1 mol % of Laurdan, respectively. All spectra acquisitions were repeated three times.

Deconvolution analysis and the solvent model

The fitting parameters were carefully selected based on considerations related to mixed solvent systems. First, a deconvolution analysis was performed as follows:

1. The second-derivative approach was performed to get the candidate peaks.
2. The asymmetric fitting equation was used for the deconvolution following a previous report (4).
3. Peaks with relative areas under curve of less than 3 % was regarded as making no contribution to the entire spectrum and were eliminated.
4. Some candidate peaks were selected from those with the highest R^2 values.

Consequently, the fitting parameters for the solvent systems were obtained empirically, such as the number of components in the solvent system, the peak positions, and the full width at half maximum (FWHM). The dielectric constants of each solvent system were measured using a dielectric probe kit (Model 85070C and a PNA-L Network Analyzer Model N5230C from Agilent Technologies, Santa Clara, CA, USA).

The deconvolution in the mixed system of acetone–hexane, hexane-ethanol, and ethanol–water were calculated with single or double fitting components. A comparison of the R^2 values of the single and double component deconvolutions are shown in Figure S8.

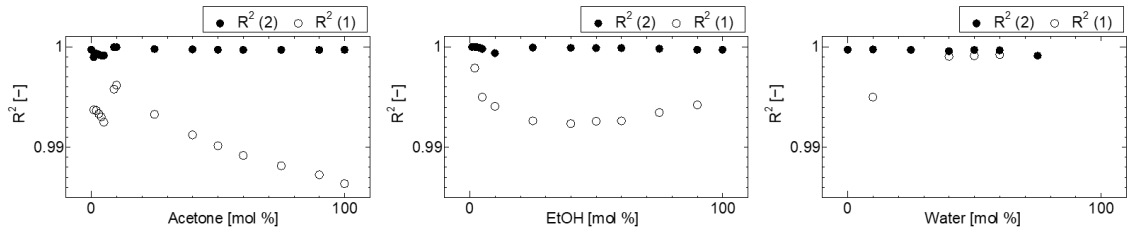

Figure S8. Comparison of the R^2 values in the acetone–hexane (left), hexane-ethanol (middle), and ethanol–water (right) systems. The R^2 values deconvoluted with two components and single components are represented as R^2 (2) and R^2 (1), as shown in the legend, respectively.

According to the higher R^2 values of deconvolutions with two components in Figure S8, the results obtained with two-component deconvolution fitting were discussed. The peak position and the FWHM of each component are summarized in Figure S9. Each point corresponds to the plot shown in Figure S10.

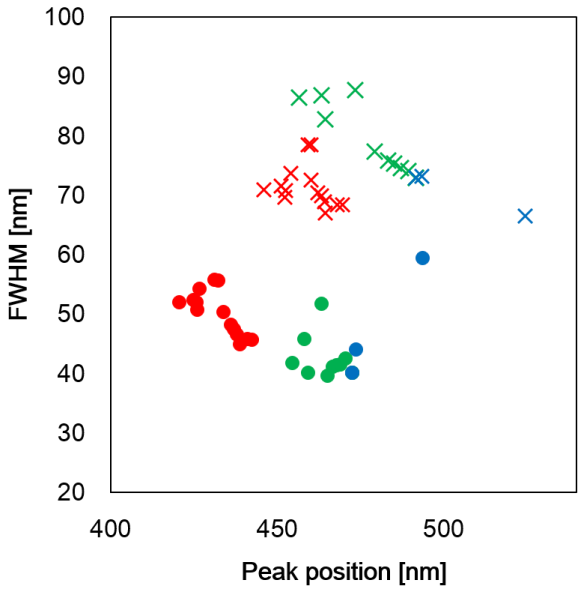

Figure S9. Summary of the correlation between emission peak position and FWHM for each deconvoluted peak. Red: hexane–acetone system; green: hexane–ethanol system; blue: ethanol–water system. The main deconvolution components are represented by filled circles, and the relaxed components were marked with crosses.

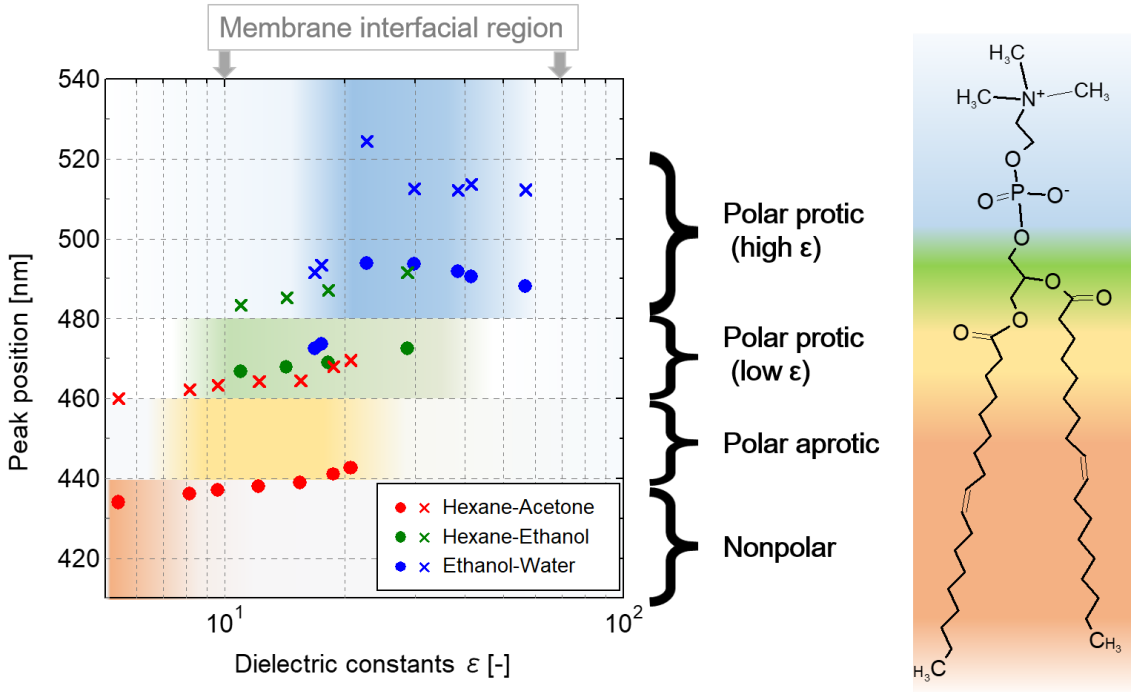

Figure S10. (Left) Correlation between the dielectric constants and the deconvoluted peak position. Red: hexane–acetone system; green: hexane–ethanol system; blue: ethanol–water system. The main deconvolution components are represented by filled circles, and the relaxed components are marked with crosses. The dielectric constants (ε) were measured using a dielectric probe kit. The interfacial region of the membrane was colored in the corresponding ε values (ε; 10 ~ 70), as reported previously (5). (Right) Chemical structure and corresponding dielectric constants for DOPC, according to the schematic diagram for egg PC (6).

The correlation between the emission peak and the dielectric constants and emission peak positions were red-shifted in the following order: hexane–acetone, hexane–ethanol, and ethanol–water (Figure S10). The shifts of peak position as a function of the dielectric constant indicated similar dependencies in any solvent system. The peak positions were stable with a wide range of dielectric constants. The two components found in a solvent system showed different FWHM values, and the one component with larger FWHM had a longer emission wavelength compared with another component (Figure S9). This broad and red-shifted component could be found even at a very low dielectric constant ($\varepsilon < 5$), indicating that this component was in a relaxed state not only because of the solvent but also due to undefined environmental factors, such as heat, collision, and reorientation. Laurdan and Prodan have two excitation states in a homogeneous solvent system, as suggested by the existence of two

lifetimes (7–9). Hence, the deconvolution with two components in a solvent system is consistent with previous finding (10).

The deconvolution of Laurdan spectra in the lipid bilayer was performed using the same procedure for solvent systems explained previously. After deconvolution, four types of peak positions were finally resulted from all of lipid bilayer systems through the temperature ranges tested in this work (Figure 5B), wherein the peaks 1, 2, 3 and 4 were observed at less than 440 nm, 440 ~ 460 nm, 460 ~ 480 nm and greater than 480 nm, respectively. The values of peak position and FWHM observed in the solvent system serve as reference boundaries for the peak positions ($420 < \lambda < 540$ nm) and FWHM ($30 < FWHM < 90$ nm), respectively (Figure S9). FWHM values for the deconvolution results in lipid bilayers are shown in Figure S11. These results suggest that the deconvoluted components of Laurdan spectra in lipid bilayers can be assigned to those in solvent systems. The number of components was changed from four to three when the R^2 value of the deconvolution with three components reached the value of the deconvolution with four components in the trial. Moreover, the amplitude of the first component located at the shorter wavelength was small to negligible. Most of the obtained spectra showed that the value of the asymmetry at half-maximum was approximately 1, which indicates that most of the deconvolution spectra were nearly symmetrical. The deconvolution based on the solvent model can be explained with the symmetric Gaussian function (10). The procedure for the deconvolution analysis is summarized in Scheme 1.

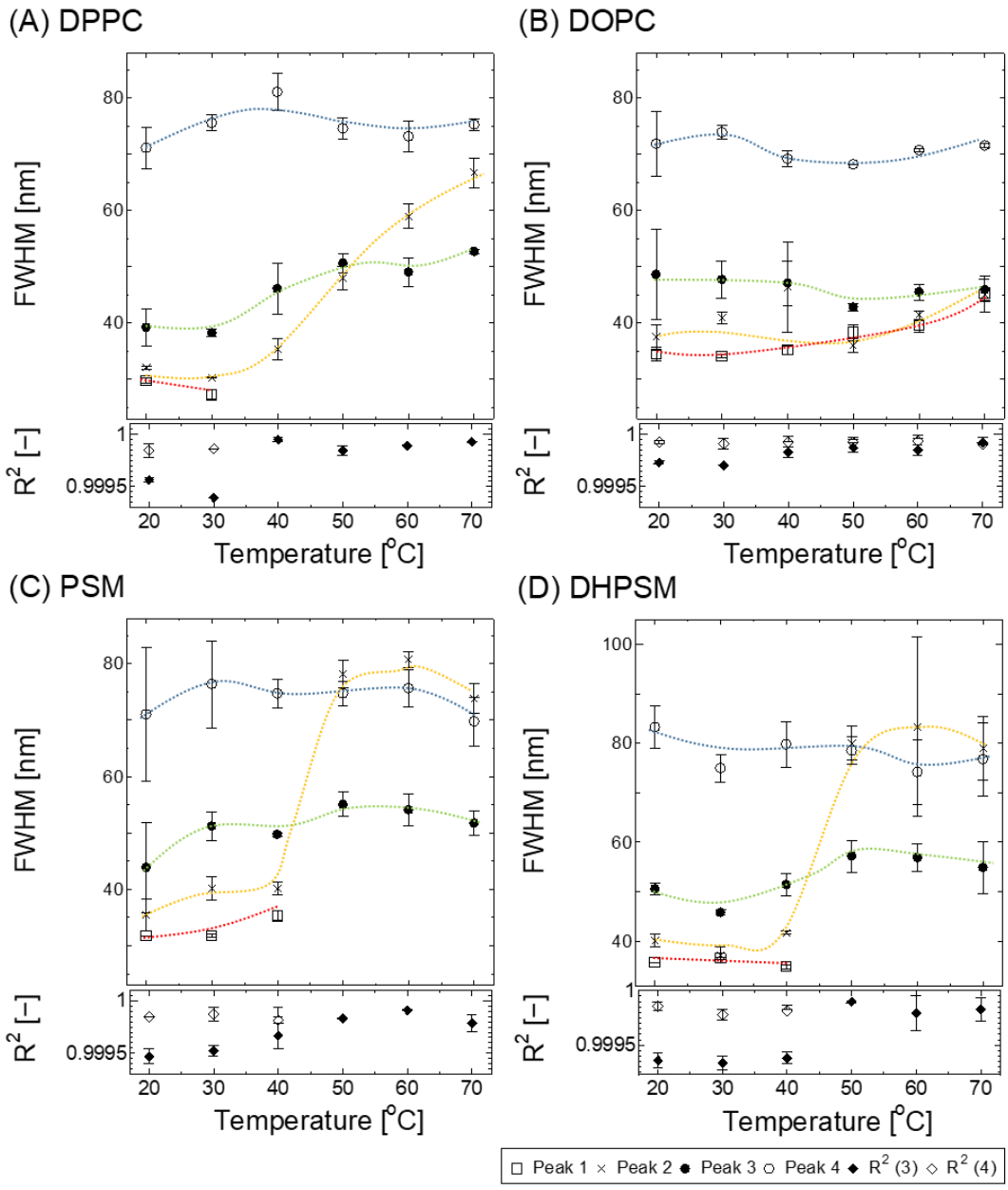

Figure S11. Summary of the FWHM of deconvolution results in lipid bilayers: (A) DPPC, (B) DOPC, (C) PSM, and (D) DHPSM. The red, yellow, green, and blue lines correspond to the components of the nonpolar (Peak 1), the polar aprotic (Peak 2), the polar protic with low ε (Peak 3), and the polar protic with high ε (Peak 4), respectively. The R^2 values are shown in each bottom panel. Solid diamonds represent R^2 values analyzed with three deconvolution curves, and open diamonds represent those analyzed with four curves, respectively. Error bars represent SEM.

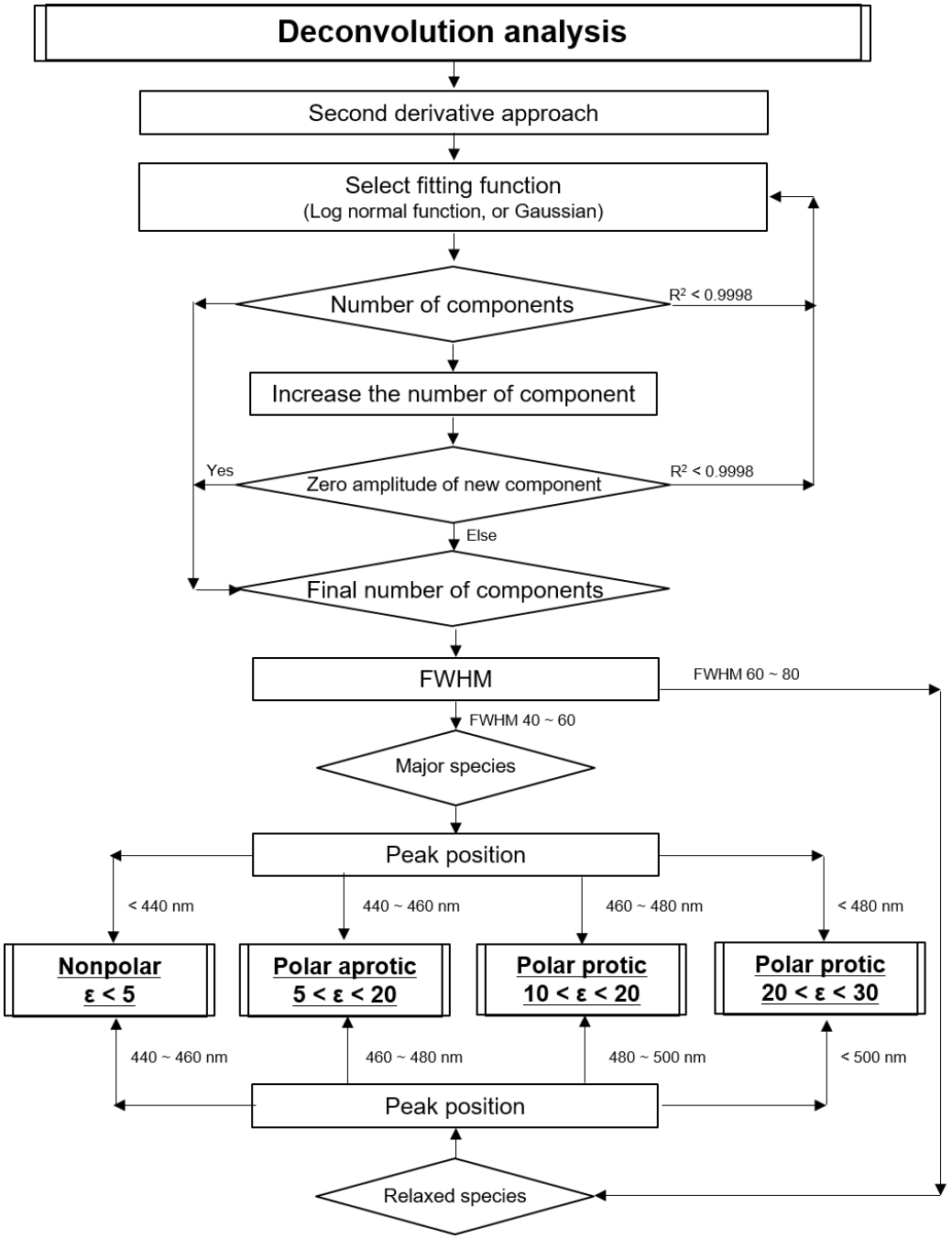

Scheme 1. Deconvolution analysis procedure.

Plausible molecular model above T_m

The molecular model relations above T_m are illustrated. Since the fluorescence behavior observed after phase transition was similar in the DPPC, PSM, and DHPSM bilayers, the model could be illustrated as shown below.

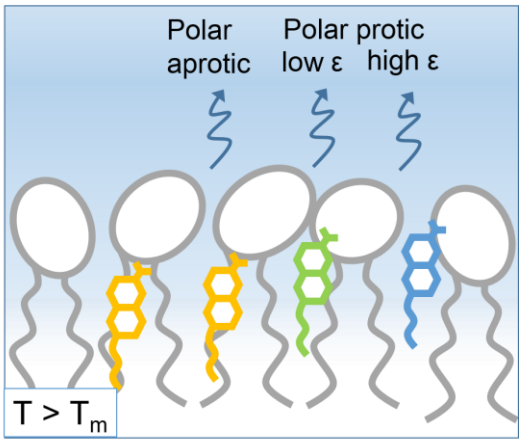

Figure S12. Molecular model above T_m for the DPPC, PSM, and DHPSM bilayers. The colors of the Laurdan are illustrated with the corresponding color in Figure 5: yellow for the polar aprotic, green for the polar protic with low ε, and blue for the polar protic with high ε.

Supporting References

1. Parasassi, T., G. De Stasio, G. Ravagnan, R.M. Rusch, and E. Gratton. 1991. Quantitation of lipid phases in phospholipid vesicles by the generalized polarization of Laurdan fluorescence. Biophys. J. 60: 179–189.

2. Chattopadhyay, A., and E. London. 1987. Parallax method for direct measurement of membrane penetration depth utilizing fluorescence quenching by spin-labeled phospholipids. Biochemistry. 26: 39–45.

3. Abrams, F.S., and E. London. 1993. Extension of the parallax analysis of membrane penetration depth to the polar region of model membranes: Use of fluorescence quenching by a spin-label attached to the phospholipid polar headgroup. Biochemistry. 32: 10826–10831.

4. Bacalum, M., B. Zorilă, and M. Radu. 2013. Fluorescence spectra decomposition by asymmetric functions: Laurdan spectrum revisited. Analytical Biochemistry. 440: 123–129.

5. Cevc, G. 1987. How membrane chain melting properties are regulated by the polar surface of the lipid bilayer. Biochemistry. 26: 6305–6310.

6. Coster, H.G.L., T.C. Chilcott, and A.C.F. Coste. 1996. Impedance spectroscopy of interfaces, membranes and ultrastructures. Bioelectrochem Bioenerg. 40: 79–98.

7. Lakowicz, J.R., and A. Balter. 1982. Analysisofexcited-state processes by phase-modulation fluorescence spectroscopy. Biophys. Chem. 16: 117–132.

8. Lakowicz, J.R., and A. Balter. 1982. Differential-wavelength deconvolution of time-resolved fluorescence intensities - a new method for the analysis of excited-state processes. Biophys. Chem. 16: 223–240.

9. Rowe, B.A., C.A. Roach, J. Lin, V. Asiago, O. Dmitrenko, and S.L. Neal. 2008. Spectral Heterogeneity of PRODAN Fluorescence in Isotropic Solvents Revealed by Multivariate Photokinetic Analysis. The Journal of Physical Chemistry A. 112: 13402–13412.

10. Vequi-Suplicy, C.C., K. Coutinho, and M.T. Lamy. 2015. New Insights on the Fluorescent Emission Spectra of Prodan and Laurdan. Journal of Fluorescence. 25: 621–629.